

---

# T-METASET: TASK-AWARE GENERATION OF METAMATERIAL DATASETS BY DIVERSITY-BASED ACTIVE LEARNING

---

**Doksoo Lee**  
 Dept. of Mechanical Engineering  
 Northwestern University  
 Evanston, IL 60208  
 dslee@northwestern.edu

**Yu-Chin Chan**  
 Siemens Corporate Technology  
 Princeton, New Jersey 08540  
 yu-chin.chan@siemens.com

**Wei (Wayne) Chen**  
 Dept. of Mechanical Engineering  
 Northwestern University  
 Evanston, IL 60208  
 wei.wayne.chen@northwestern.edu

**Liwei Wang**  
 School of Mechanical Engineering  
 Shanghai Jiao Tong University  
 Shanghai, P.R. China, 200240  
 iridescence@sjtu.edu.cn

**Anton van Beek**  
 School of Mechanical and Materials Engineering  
 University College Dublin  
 Belfield, Dublin 4, Ireland, D04 V1W8  
 anton.vanbeek@ucd.ie

**Wei Chen\***  
 Dept. of Mechanical Engineering  
 Northwestern University  
 Evanston, IL 60208  
 weichen@northwestern.edu

## ABSTRACT

Inspired by the recent success of deep learning in diverse domains, data-driven metamaterials design has emerged as a compelling design paradigm to unlock the potential of multiscale architecture. However, existing model-centric approaches lack principled methodologies dedicated to high-quality data generation. Resorting to space-filling design in shape descriptor space, existing metamaterial datasets suffer from property distributions that are either highly imbalanced or at odds with design tasks of interest. To this end, we propose t-METASET: an intelligent data acquisition framework for task-aware dataset generation. We seek a solution to a commonplace yet frequently overlooked scenario at early design stages: when a massive ( $\sim O(10^4)$ ) shape library has been prepared with no properties evaluated. The key idea is to exploit a data-driven shape descriptor learned from generative models, fit a sparse regressor as the start-up agent, and leverage diversity-related metrics to drive data acquisition to areas that help designers fulfill design goals. We validate the proposed framework in three hypothetical deployment scenarios, which encompass general use, task-aware use, and tailororable use. Two large-scale shape-only mechanical metamaterial datasets are used as test datasets. The results demonstrate that t-METASET can incrementally grow task-aware datasets. Applicable to general design representations, t-METASET can boost future advancements of not only metamaterials but data-driven design in other domains.

**Keywords** Data acquisition · Data-driven design · Active learning · Variational autoencoder · Gaussian processes · Determinantal Point Processes · Metamaterials

## 1 Introduction

Metamaterials are artificially architected structures that support unusual properties from their structure rather than composition [1]. The recent advancements of computing power and manufacturing have fueled research on

---

\*Corresponding author: Wei Chen (weichen@northwestern.edu)

metamaterials, including theoretical analysis, computational design, and experimental validation. Over the last two decades, outstanding properties achievable by metamaterials have been reported from a variety of fields, such as optical [2], acoustic [3], thermal [4], and mechanical [5]. They have been widely deployed to new applications in communications, aerospace, biomedical, and defense, to name a few [6]. From a design point of view, leveraging the rich designability in the hierarchical systems is key to further disseminating metamaterials as a versatile material platform, which not only realizes superior functionalities but also facilitates customization and miniaturization. To this end, there has been growing demand for advanced design methods to harness the potential of metamaterials.

Data-driven metamaterials design (DDMD) offers a route to intelligently design metamaterials. In general, the approaches build on three main steps: data acquisition, model construction, and inference for design purposes. DDMD typically starts with a precomputed dataset that includes a large number of structure-property pairs [7, 8, 9, 10, 11]. Machine learning model construction follows to learn the underlying mapping from structure to property, and sometimes vice versa. Then the data-driven model is used for design optimization, such as at the “building block” or unit cell level, and optionally tiling in the macroscale as well when aperiodic designs are of interest. The key distinctions of DDMD against conventional approaches are that (i) DDMD can accommodate domain knowledge (in both dataset and model) with topologically free design variation; (ii) it has little restrictions on analytical formulations of design interest; (iii) some of DDMD enables iteration-free design, which pays off the initial cost of data acquisition and model construction. Capitalizing on the advantages, DDMD has reported a plethora of achievements in recent years from diverse domains [1, 8, 9, 10, 12, 13, 14].

Despite the recent surge of DDMD, sufficient attention has not been given to data acquisition and data quality assessment – the very first step of DDMD. In data-driven design, *dataset is a design element*; a collection of data points forms a landscape to be learned by a model, which is an “abstraction” of the data, and to be explored by either model inference or modern optimization methods. Hence, data quality always ends up *propagating* into the subsequent stages. Yet the downstream impact of naive data acquisition is opaque to diagnose and thus challenging to prevent *a priori*. Underestimating the risk, common practice in DDMD typically resorts to a large number of space-filling designs in the shape space spanned by the shape parameters. This *inevitably* hosts imbalance – distributional bias of data – in the property space [15, 16, 11, 17] formed by the property vectors. The succeeding tasks involving a data-driven model – training, validation, and deployment to design – follow mostly without rigorous assessment on data quality in terms of diversity, design quality, feasibility, *etc*. The practice overlooks not only *data imbalance itself* but also *the compounding ramifications* at the design stage.

Taking data imbalance as the fundamental hurdle to successful deployment of DDMD, we propose *task-aware* METASET (t-METASET): as an extension of our former work METASET [11] with special attention to starting with sparse observations for increased efficiency. t-METASET builds a sequential data acquisition framework building on data-driven shape descriptor, recursive model update, and metric-based active learning. In this study, “task-aware” approaches are supposed to rate individual datapoints based on the utility for a given *specific* design scenario, rather than on distributional metrics (*e.g.* diversity) for *general* use. The framework handles data bias reduction (for generic use) and design quality (for particular use) simultaneously, by leveraging diversity and quality as the sampling criteria, respectively. We advocate that (i) building a good dataset should be an *iterative* procedure; (ii) diversity-driven sampling [18] can efficiently suppress the property imbalance of multi-dimensional regression that most DDMD is involved with [11]; (iii) property diversity significantly improves fully aperiodic metamaterial designs, as have been shown by recent reports [15, 19, 20, 21]. Distinct from existing work, however, we primarily seek a solution to an commonplace – yet frequently overlooked – scenario that designers face during data preparation: we wish to collect or generate a large-scale shape dataset *without any property evaluated at the start*, while also aiming to acquire a uniform or a controlled task-aware property/shape distributions. To achieve this goal, an intuitive method is to evaluate the properties of all the designs *a priori*, then downsample a balanced subset based on diversity or task-related quality, as presented by Y. C. Chan *et al.* [11]. We propose that taking the opposite approach improves the efficiency and generality of data acquisition: our t-METASET incrementally “grows” a high-quality dataset from sparse property information, which is not only diverse but also task-aware. Figure 1 illustrates a schematic of the t-METASET procedure. The central ideas are (i) to extract a compact shape descriptor for microstructures by learning from a shape-only microstructure (building block) dataset, (ii) to sequentially update a sparse regressor, *e.g.*, Gaussian process (GP), as a start-up “agent” that efficiently learns the nonlinear shape-property mapping with *sparse* observations, and (iii) to intelligently curate samples based on batch sequential metric-based sampling [18], accommodating shape diversity, *estimated* property diversity, and user-defined quality.

In the context of DDMD, the key intellectual contributions of t-METASET are three-fold:

- t-METASET offers a principled framework on how to build a balanced dataset *at the start-up stage*, with rigorous metrics and minimal heuristics, without property being evaluated at the beginning,
- t-METASET provides a solution to *property bias* prevalent in existing metamaterial datasets,

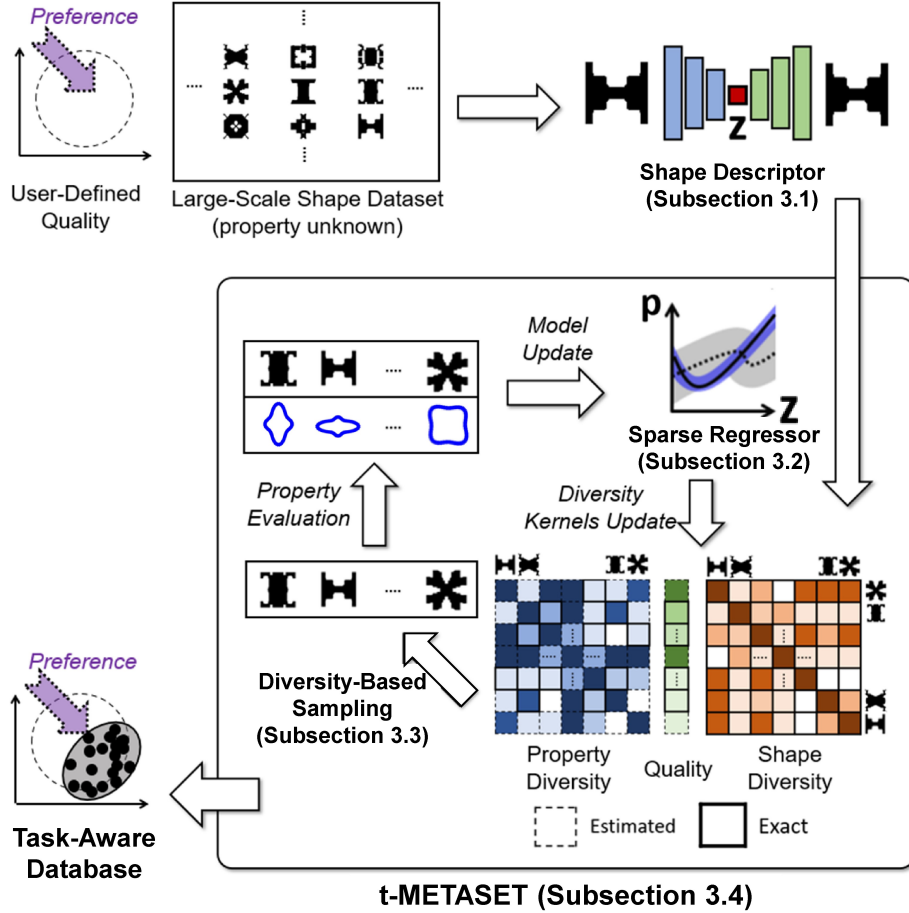


Figure 1: An overview of t-METASET. Given a shape-only dataset, a compact shape descriptor of microstructures is distilled by a generative model. Taking the shape descriptor as the input, a sparse regressor efficiently learns the nonlinear shape-property mapping with sparse observations. Building on the property prediction over unseen shapes, diversity-driven sampling serves as the decision maker that hinges on shape diversity, property diversity (estimated by the regressor), and optionally user-defined quality. Once evaluated, a new batch of structure-property pairs is passed to the regressor to refine its prediction. The t-METASET framework helps designers achieve a task-aware dataset by suppressing undesirable distributional bias and enforcing desirable one.

- t-METASET can produce *task-aware* datasets, whose distributional characteristics can be tailored according to user-defined design tasks.

We argue the advantages of t-METASET are: (i) scalability, (ii) modularity, (iii) data customizability, (vi) no restrictions on shape generation schemes, (v) no dependency on domain knowledge and, by extension, (vi) wide applicability over generic metamaterial datasets. We validate t-METASET with two large-scale shape only mechanical metamaterial datasets (containing 88,180 and 57,000 metamaterial shapes, respectively) that are built from different ideas, without preliminary downsampling of the massive groundsets or arduous parameter tuning. The validation involves three scenarios assuming different sampling criteria: (i) considering only diversity aiming at *general use* (global metamodeling), (ii) considering quality-weighted diversity aiming at *task-aware use*, and (iii) considering shape-property joint diversity for *tailorable use*.

## 2 Property Bias Induced by Nearly-Uniform Sampling in Shape Space

Property bias prevails in existing metamaterial datasets. To convey this point, we examine an example of a lattice-based 2-D mechanical metamaterial dataset. Lattice based metamaterials have been intensely studied due to their outstanding

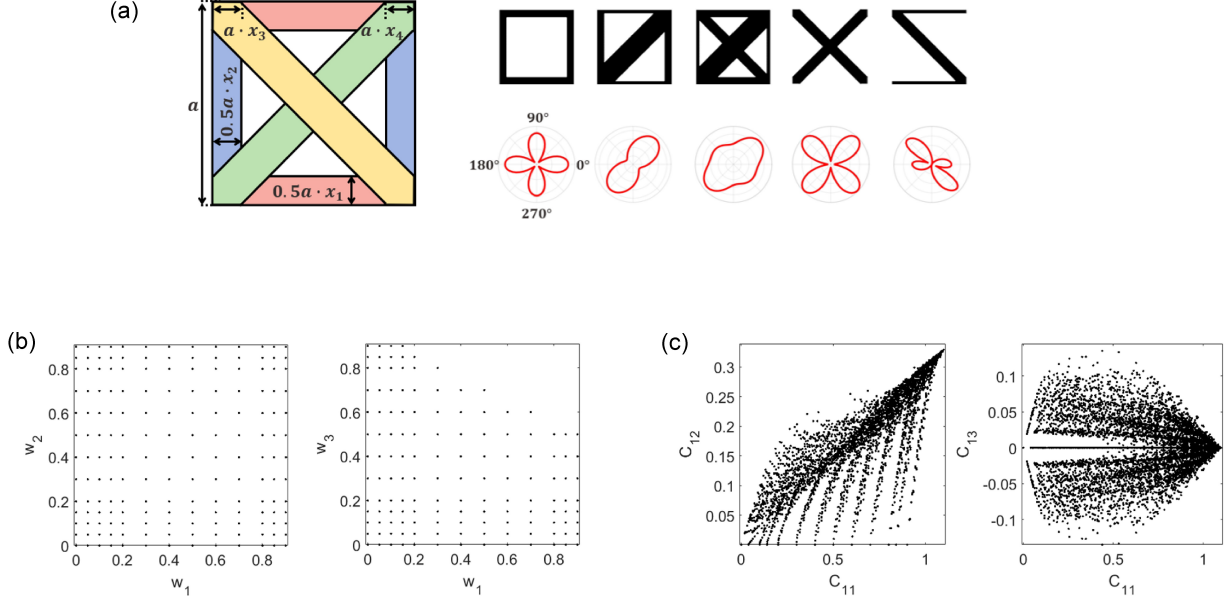


Figure 2: Illustration on  $\mathcal{D}_{lat}$  [15]. (a) Shape generation method: (left) shape representation; (top right) examples of generated geometries; (bottom right) the resulting surfaces of elastic modulus. (b) Data distribution in projected parametric shape space (thickness of each bar group). (c) Data distribution in projected property space.

performance-to-mass ratio, great heat dissipation, and negative Possion's ratio [1]. L. Wang *et al.* devised a lattice-based dataset, called  $\mathcal{D}_{lat}$  in this work [15]. In the dataset, a unit cell geometry (*i.e.* microstructure, building block) takes six bars aligned in different directions as its geometric primitives (see Figure 2(a) for illustration). All unit cells can be fully specified by four parameters associated with the thickness of each bar group. The shape generation scheme produces diverse geometric classes (*i.e.* baseline, family, motif, basis, and template), as exemplified classes in Figure 2(a). Each shape class exhibits different topological features, which offer diverse modulus surfaces of homogenized properties ( $C_{11}, C_{12}, C_{13}, C_{22}, C_{23}, C_{33}$ ). Figure 2(a) displays that nearly uniform sampling in the parametric shape space  $\Omega_w = [0, 1]^4$  is used for data population. We examine the non-trivial microstructures, except both solid ( $v_f = 1$ ) or void ( $v_f = 0$ ); this explains why some of the regions in Figure 2(b) and (c) have no datapoints. In the original reference, the dataset was used for the natural frequency maximization problem as a case study of the generalized de-homogenization method proposed.

Herein, we look into the data distribution of  $\mathcal{D}_{lat}$ , presented in Figure 2. The nearly uniform sampling used for the data generation ensures good uniformity in the parametric shape space (Figure 2(b)). On the other hand, the corresponding property distributions in Figure 2(c) show considerable imbalance, which epitomizes that *data balance in parametric shape space does not ensure that in property space*. By extension, we argue that such property imbalance is prevalent in many metamaterial datasets generated by space-filling design in parametric shape space [16, 11, 17, 22, 23]. We claim that: (*i*) *any* metamaterial dataset collected based on naive sampling in parametric shape space are subject to *substantial* property bias [16, 11, 17, 22, 23], and more importantly, (*ii*) this is highly likely to hold true for datasets with generic design representations – other than parametric ones – as well [11, 19, 10, 24, 25]. The general statement in part is grounded on the near-zero correlation between shape similarity and property similarity in large-scale metamaterial datasets ( $\sim O(10^4)$ ), consisting of microstructures represented as pixel/voxel, reported by Y. C. Chan *et al.* [11]. Overlooking the significant property imbalance, many methods assume that the subsequent stages of DDMD can accurately learn and perform inference under strong property imbalance, ignoring the compounding impact of data bias [26].

Property bias is *inevitable* without supervision. Properties – a function of a given shape – are unknown before evaluation. Obtaining their values is the major computational bottleneck, not only at the data preparation stage but also in the whole DDMD pipeline. The worst case would be: one evaluates all the shape samples with time-consuming numerical analysis (e.g., finite element analysis (FEM); wave analysis) and trains a model on the data, only to end up with a property distribution that is severely biased outside where one had planned to deploy the data-driven model. To circumvent such unwanted scenarios, it is necessary to monitor property bias at early stages, and maneuver the sampling process in a

supervised manner, *during* data acquisition, not after. As a solution, we propose t-METASET: a sequential task-aware data acquisition framework with systematic bias control.

### 3 Proposed Method

In this section, we walk through the three components of the proposed t-METASET: shape descriptor (Section 3.1), sparse regressor (Section 3.2), and diversity-driven sampling (Section 3.3). Then the whole algorithm as its entirety is presented. (Section 3.4)

#### 3.1 Shape Descriptor

The shape space of discretized metamaterial systems is extremely high-dimensional due to the need to represent free-form shape variations. Exploring or sampling the entire high-dimensional shape space is expensive and computationally unaffordable. Therefore, we need to extract compact shape descriptors as a lower-dimensional vector representation of shapes to enable efficient shape space exploration or sampling.

In the literature of DDMD, shape descriptors roughly fall into three categories: physical descriptors, spectral descriptors, and data-driven descriptors. First, physical descriptors represent a geometry based on geometric features of interest, such as curvature, moment, angle, shape context, etc [27]. Hence, the key advantage is high interpretability provided by the physical criteria. For example in DDMD, Y. C. Chan *et al.* [11] employed the division point-based descriptor [28]. The method recursively identifies centroids of a given geometry at several granularity levels, and concatenates the coordinate components to form the shape descriptor. The 124-D descriptor was used for measuring shape similarity that enables diversity-driven sampling. Second, spectral descriptors exploit spectral decomposition of shape. Z. Liu *et al.* [29] proposed a Fourier transform based descriptor as a topological encoding method for optical metasurfaces. The key idea is to harness Fourier transform of level-set functions – high-dimensional embedding of given binary images – as a sparse shape descriptor, which offers representational parsimony, reconstruction capability (inverse Fourier transform), efficient symmetry handling, and continuous latent space. The efficacy was demonstrated by inverse optimization for non-paraxial diffractive optical elements. Third, data-driven descriptors exploits automatic feature engineering driven by data. L. Wang *et al.* [10] employed variational autoencoder (VAE) [30] as a deep generative model for DDMD. It was demonstrated that the latent representation serves as a compact shape similarity measure in light of given data, facilitates interpolation across microstructures, and encodes interpretable geometric patterns as well. The versatility was demonstrated via iteration-free inverse design of unit cells, metamaterial family design, and data-driven multiscale TO for shape morphing.

In this work, we employ the latent representation of VAE as our shape descriptor. VAE is a generative model trained by unsupervised learning [30]. Figure 3(a) offers a schematic of shape VAE used in our study. The VAE builds on two key components, encoder  $E$  and decoder  $G$ . Assuming the input instance is an image, the encoder involves a set of progressively contracting layers to capture underlying low-dimensional features, until it reaches the bottleneck layer, which provides the latent vector as  $z = E(\phi(x, y))$  where  $\phi(x, y)$  is the signed distance field (SDF) of a binary microstructure image  $I(x, y)$ . The decoder, reversely, takes a latent variable from the information bottleneck and generates a reconstructed image as  $\hat{\phi}(x, y) = G(z)$ .

We advocate the VAE descriptor as the shape descriptor of metamaterial unit cells based on three aspects. First, our primary interest in VAE is the low-dimensional latent space that is distilled from the complex geometries and efficiently encodes the most salient features of microstructures. The dimensional parsimony is crucial to make a sparse regressor have compact yet expressive predictors and to expedite the subsequent diversity-based sampling. Second, this work also takes advantage of the distributional regularization imposed on the encoder: the latent vectors are enforced to roughly be multivariate Gaussian. This offers built-in scaling across individual components of the latent representation, as a byproduct of the VAE training. The component-wise balance makes diversity-based sampling robust to arbitrary scaling. Lastly, transformation variance of the latent descriptor is necessary for mechanical design to build a structure-property mapping that recognizes transformation, so that different shape descriptors representing a single microstructure under transformations (e.g., scaling and rotation) can be linked into different properties.

We introduce key formulations of VAEs. A VAE assumes that given data, formatted as a SDF  $\phi(x, y) \in \mathcal{S}$  in this study, have come from an underlying random process specified by a latent variable  $z$ . Each instance  $\phi$  and latent variable  $z$  are viewed a realization of the conditional distribution  $p_\theta(\phi|z)$  and prior distribution  $p_\theta(z)$ , respectively, where  $\theta$  is the parameters that specifies the distributions. The marginal likelihood of a given instance  $\phi$  reads:

$$\log p_\theta(\phi) = KL[q_\psi(z|\phi)||p_\theta(z|\phi)] + \mathcal{L}(\theta, \psi; \phi), \quad (1)$$

where  $KL[\cdot||\cdot]$  is the Kullback-Leibler divergence as a non-negative distance measure between two distributions;  $q_\psi(z|\phi)$  is the variational posterior that is specified by the parameter  $\psi$  and approximates the true posterior  $p_\theta(z|\phi)$

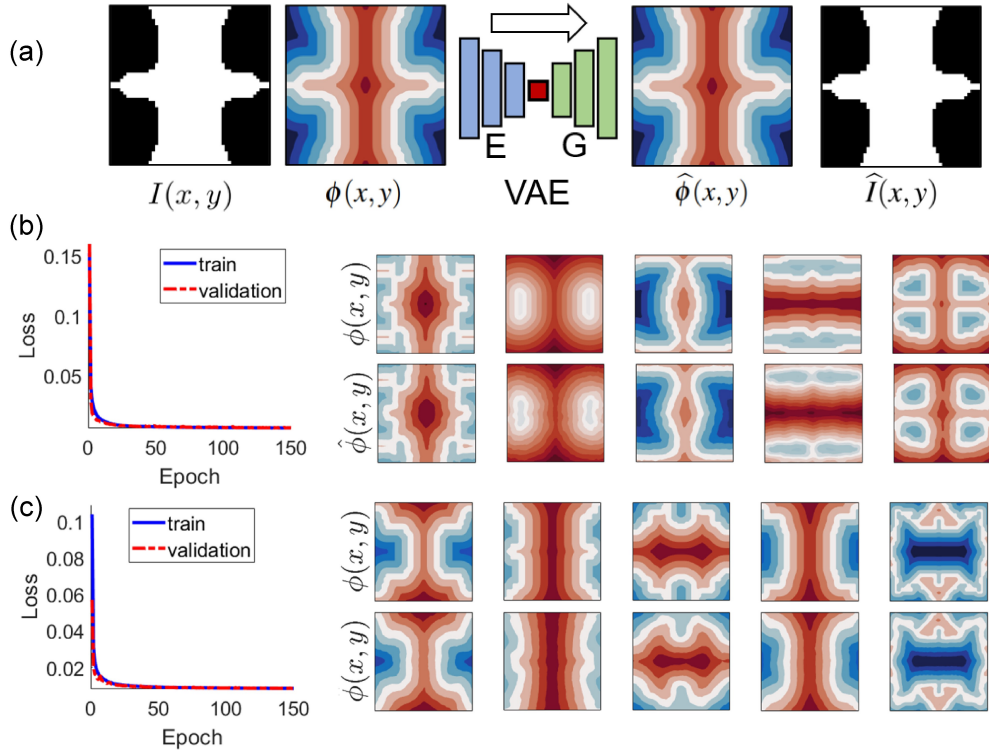


Figure 3: Shape VAE. (a) Schematic of the architecture. (b) The training result of  $\mathcal{D}_{mix}$ . (c) The training result of  $\mathcal{D}_{TO}$ .

to bypass the intractability of the marginal distribution [30]; and  $\mathcal{L}(\cdot)$  is the variational lower bound on the marginal likelihood. Usual practice for training is to rearrange the equation and to maximize the evidence lower bound:

$$\mathcal{L}(\theta, \psi; \phi) = -KL[q_\psi(z|\phi)||p_\theta(z|\phi)] + \mathbb{E}_{q_\psi(z|\phi)}[\log(p_\theta(\phi|z))]. \quad (2)$$

The first right-hand side term  $KL[\cdot||\cdot]$  involves the regularization loss that enforces the latent variable  $z$  to be distributed as multivariate Gaussian, while the second term denotes the reconstruction loss. The approximated lower bound allows stochastic gradient decent to be used for end-to-end training of the whole VAE. For efficient training, standard VAE assumes the prior distribution as  $p_\theta(z) \sim \mathcal{N}(\mathbf{0}, \mathbf{I})$  and the variational posterior as  $q_\psi(x|z') \sim \mathcal{N}(\mu, \sigma^2)$ , respectively. Herein, the reparameterization trick [30] involves a stochastic embedding  $z'$  as  $z' = \mu + \sigma \odot \epsilon$  with a noise  $\epsilon \sim \mathcal{N}(\mathbf{0}, \mathbf{I})$ . The training boils down to the following optimization problem:

$$\min_{\theta, \psi} [-\mathcal{L}(\theta, \psi; \phi)] = \frac{1}{|\mathcal{S}|} \sum p_\theta(\phi|z') - \frac{1}{2} \sum [1 + \log(\sigma^2) - \sigma^2 - \mu^2], \quad (3)$$

where  $|\mathcal{S}|$  is the number of data.

Figure 3(b) and (c) report the VAE training results of each dataset, 2-D multiclass blending dataset ( $\mathcal{D}_{mix}$ ) [19] and 2-D topology optimization dataset ( $\mathcal{D}_{TO}$ ) [31, 32], respectively. Concise description of the datasets can be found in Section 4.1. All binary images of microstructures  $I(x, y)$  are converted into SDFs  $\phi(x, y)$  to facilitate VAE training (Figure 3(a)) [33, 34, 29]. The VAE architecture was set based on that in L. Wang *et al.* [10]. The dimension of latent space is set as 10, with the trade-off between dimensionality and reconstruction error taken into account. Adam optimizer [35] was used under training the VAE with the following setting: learning rate  $10^{-4}$ , batch size 128, epochs 150, and dropout probability 0.4. Each shape dataset is split into training set and validation set with the ratio of 80% and 20%, respectively. In Figure 3(b) and (c), each training history shows stable convergence behavior for both training and validation. From the plots of SDF instances on the right side, we qualitatively confirm good agreement between the input instances (top) and their reconstruction (bottom), for both training results.

### 3.2 Sparse Regressor

#### 3.2.1 Gaussian Processes

In t-METASET, a sparse regressor is an essential pillar that enables active learning and task-aware distributional control under epistemic uncertainty (*i.e.* lack of data). We implement a GP regressor as the “agent” in this work. The mission is to learn the underlying structure-property mapping from sparse data, and to provide predictions over unseen shapes as  $\hat{p} = \mathcal{GP}(z)$  in batch sequential sampling. In this study, the GP takes the VAE latent shape descriptor as its inputs, which offers substantial dimension reduction ( $50^2\text{-D} \rightarrow 10\text{-D}$  in this work). We advocate a GP as the sparse agent due to three key advantages: (*i*) model parsimony congruent with sparse data; (*ii*) decent modeling capacity of highly nonlinear structure-property regression (*i.e.*  $z \rightarrow p$ ); (*iii*) roughness parameters as an indicator of model convergence, to be used for sampling mode transition (detailed in Section 3.2.2).

Building on the advantages of the GP, our novel idea on task-aware property bias control is to (*i*) construct an *estimated* property similarity kernel  $\widehat{L}_p$  (Section 3.3.1) from the GP prediction  $\hat{p} = \mathcal{GP}(z)$ , as the counterpart of the shape kernel  $\widehat{L}_s$  and (*ii*) employ conditional Determinantal Point Processes (DPP) [18] – a diversity-based sampling approach – over the estimated property kernel  $\widehat{L}_p$  to sample a batch based on expected property diversity. The property kernel  $\widehat{L}_p$  estimates property similarity, *prior to design evaluation*, not only between train-train pairs, but also train-unseen and unseen-unseen ones. In this way, t-METASET intelligently curates a batch  $\mathcal{B}$  hinging on both (estimated) property diversity and (exact) shape diversity. It is important to note that, at an incipient phase, we do not rely on  $\widehat{L}_p$ , as the predictive performance of a multivariate multiresponse GP ( $\mathbb{R}^{D_z} \rightarrow \mathbb{R}^m$ , where  $m$  is the property dimensionality) trained on tiny data is not reliable. We determine the turning point – when to start to respect the GP prediction – based on the convergence history of a set of the GP hyperparameters: roughness parameters (*i.e.* scale parameters).

As a background to the roughness parameters, we introduce key formulations of GPs. A GP is a collection of random variables, any of whose finite subset is distributed as multivariate Gaussian [36]. Given a set of observations, a GP with  $m$  responses is fully specified by its mean and covariance functions as

$$f \sim \mathcal{GP}(\mu(z), \text{cov}(z, z')), \quad (4)$$

where  $\mu(\cdot)$  is the mean function;  $\text{cov}(\cdot, \cdot)$  is the covariance function;  $f$  is a function viewed as a realization from the underlying distribution. For the multivariate input  $z$  and the multiresponse outputs  $p$  in our study, the covariance function reads:

$$\text{cov}(z, z') = \Sigma \otimes r(z, z') \quad (5)$$

where  $\Sigma$  is the  $m \times m$  dimensional multiresponse prior variance,  $\otimes$  is the Kronecker product, and  $r(\cdot, \cdot)$  is the correlation function. In this work we use the squared exponential correlation function given as

$$r(z, z') = \exp(-(z - z')\Theta(z - z')) \quad (6)$$

where  $\Theta = \text{diag}(10^\omega)$  and  $\omega = [\omega_1, \omega_2, \dots, \omega_{d_z}]^T$  is the roughness parameters [37]. Given a dataset  $\mathcal{D} = \{(\mathbf{z}, \mathbf{p})\} = \{(z_i, p_i)\}_{i=1}^n$ , fitting a multi-response GP regressor is equivalent to finding an optimal point estimate of the hyperparameters that maximize the Gaussian likelihood function:

$$[\widehat{\beta}, \widehat{\Sigma}, \widehat{\omega}] = \arg \min_{[\beta, \Sigma, \omega]} \left[ \frac{n}{2} \log(\det(\Sigma)) + \frac{1}{2} \log(\det(\mathbf{R})) + \frac{1}{2\sigma^2} (\mathbf{p} - \mathbf{1}\beta)^T \mathbf{R}^{-1} (\mathbf{p} - \mathbf{1}\beta) \right] \quad (7)$$

where  $\mathbf{1}$  is an  $n \times m$  dimensional vector of ones,  $\beta = [\beta_1, \dots, \beta_m]^T$  is  $1 \times m$  dimensional vector of weights,  $\log(\cdot)$  is the natural logarithm, and  $\mathbf{R}$  is the  $n \times n$  correlation matrix with  $(i, j)^{\text{th}}$  element  $R_{ij}$  given as  $r(z_i, z_j)$  for  $i, j = 1, \dots, n$ . In the above formulation of the likelihood we have assumed a constant prior as given by  $\mathbf{1}\beta$ . More complex basis functions can be used to represent the prior mean (*e.g.*, linear, or quadratic); however, this is not advised as this information is typically not known *a priori*, and is likely to compromise model accuracy when chosen incorrectly.

After approximation of the hyperparameters, the posterior predictive distribution for an unobserved input  $z_{\text{new}}$  can be obtained by conditioning the prior distribution (*i.e.*, Eq. 5) on the observed data  $\mathcal{D}$  [38]. Specifically, the mean and the covariance of the posterior predictive distribution is given as

$$\mu(z_{\text{new}}) = \widehat{\beta} + \mathbf{r}^T(z_{\text{new}}) \mathbf{R}^{-1} (\mathbf{p} - \mathbf{1}\widehat{\beta}), \quad (8)$$

$$\text{cov}(z_{\text{new}}) = \widehat{\Sigma} \left[ r(z_{\text{new}}, z_{\text{new}}) - \mathbf{r}^T(z_{\text{new}}) \mathbf{R}^{-1} \mathbf{r}(z_{\text{new}}) + \mathbf{W}^T (\mathbf{1}^T \mathbf{R}^{-1} \mathbf{1}) \mathbf{W} \right], \quad (9)$$

where  $\mathbf{r}(z_{\text{new}})$  is an  $n \times 1$  dimensional vector whose  $i^{\text{th}}$  element is given as  $r(z_{\text{new}}, z_i)$  for  $i = 1, \dots, n$ ,  $\mathbf{W} = \mathbf{1}' - \mathbf{1}^T \mathbf{R}^{-1} \mathbf{r}(z_{\text{new}})$ , and  $\mathbf{1}'$  is a  $m \times 1$  dimensional vector of ones.

### 3.2.2 Roughness parameters

Roughness parameters  $\omega = [\omega_1, \omega_2, \dots, \omega_d]^T$  dictate fluctuation levels of responses w.r.t. each predictor (each component of  $z$  in our study), in light of given data. R. Bostanabad *et al.* [37] used the fluctuations of roughness parameters and their estimated variance to qualitatively determine if sufficient samples were collected during GP training. Building on that, we monitor the roughness parameters  $\omega$  and take the convergence of roughness parameters as a proxy for model convergence. The roughness residual serves as the transition criterion across sampling modes. We define the convergence criterion involving the roughness residual metric as follows:

$$r^{(i+1)} = \sqrt{\frac{1}{D_z} \|\omega^{(i+1)} - \omega^{(i)}\|^2} \leq \tau \quad (10)$$

where  $\tau$  is a threshold associated with the sampling mode transition. At an early stage the roughness residual exhibits a “transient” behavior. As more data are added, the residual goes to 0, implying a mild convergence of the GP. In this work, we set two different values of threshold namely,  $\tau_1 = 0.02$  and  $\tau_2 = 0.01$ . We assume each convergence criterion is met if the residuals of five consecutive iterations are below the threshold.  $\tau_1$  is to identify a mild convergence, indicated by the larger tolerance. Once met, t-METASET initiates Stage II, where estimated property diversity serves as the main sampling criterion. Meanwhile, the smaller threshold  $\tau_2$  is used to decide when to stop the GP update: as more data comes in, the variations of roughness get unnoticeable [37], whereas the computational cost of fitting the GP rapidly increases as  $\sim O(|\mathcal{D}^{(t)}|^3)$  as a consequence of having to invert the covariance matrix  $\mathbf{R}$ . We prioritize speed, with a compromise of prediction accuracy. Details of the implementation with the other pillars can be found in Section 3.4. When reporting the results of t-METASET, we will include the history of the residuals, in addition to that of diversity metrics.

## 3.3 Diversity-Based Sampling

In this section, we elaborate on diversity-based batch sequential sampling. It maneuvers the data acquisition as the *decision maker*, leveraging both the compact shape descriptor distilled by VAE (Section 3.1) and “dynamic” prediction offered by the GP agent (Section 3.2), from beginning to end of t-METASET. Recalling the mission of t-METASET – task-aware generation of balanced datasets – we advocate DPP as a diversity sampler primarily based on three key advantages as follows: (i) DPPs offer a variety of practical extensions (*e.g.* cardinality constraint, conditioning, *etc*); (ii) The probabilistic modeling from DPP captures the trade-off between diversity (datapoint efficiency in general) and quality (datapoint score w.r.t. a specific design task); (iii) Importantly, *DPPs are flexible in terms of handling distributional characteristics*: object-driven sampling approaches [39] mostly support either exploration (diversity of input) or exploitation (quality of output), while DPPs do all the combinations of diversity (input/output) and quality (shape/joint), without restrictions.

t-METASET harnesses a few extensions of DPPs. Section 3.3.1 provides fundamental concepts related to DPP. Section 3.3.2 introduces conditional DPPs that are key for DPP-based active learning, and brings up the scalability issue of large-scale similarity kernels. As a remedy, a large-scale kernel approximation scheme is introduced in Section 3.3.3. Section 3.3.4 addresses how to accommodate design quality into DPP, which enables “task-aware” dataset construction.

### 3.3.1 Similarity and DPP

In general, an instance of interest could be represented as a vector. A similarity metric between item  $i$  and  $j$  can then be quantified a monotonically decreasing function of the distance in the virtual item space as

$$s_{ij} = T(h(x_i, x_j)), \quad (11)$$

where  $s_{ij}$  is the pairwise similarity between item  $i$  and  $j$ ,  $h(\cdot, \cdot)$  is a distance function,  $T$  is a monotonically decreasing transformation: the larger a distance, the smaller the similarity is. One way to represent all the pairwise similarities of a given item set is to construct the  $n \times n$  similarity matrix  $L$  as  $L_{ij} = s_{ij}$ , where  $n = |L|$  is the set cardinality. The matrix is often called a *similarity kernel* in that it converts a pair of items into a distance measure (or similarity, equivalently). While any combinations of similarity and transformation are supported by the formalism above, usual practice favors the transformations that result in positive semi-definite (PSD) kernels for operational convenience, such as matrix decomposition. Following this, we employ Euclidean distance  $h(x_i, x_j) = \sqrt{\|x_i - x_j\|^2}$  and the square exponential transformation. The resulting similarity kernel reads:

$$L_{ij} = \exp\left(\frac{-\|x_i - x_j\|^2}{2\sigma_L^2}\right), \quad (12)$$

where  $\sigma_L$  is the lengthscale parameter (*i.e.* bandwidth) that tunes the correlation between items.

DPP provides an elegant probabilistic modeling that favors a subset composed of diverse instances [18]. DPPs have been employed for a variety of applications that take advantage of set diversity, such as recommender systems [40], summarization [41], object retrieval [42], *etc.* The defining property of DPPs is:

$$\mathbb{P}(X = A) \propto \det(A), \quad (13)$$

where  $A$  is a subset of a ground set  $\mathcal{V}$ ;  $\mathbb{P}(X = A)$  is the probability to sample  $A$ ;  $\det(\cdot)$  is the matrix determinant operation. The property has an intuitive geometric interpretation:  $\det(A)$  is associated with the hypervolume spanned by the constituent instances. If the catalogue  $A$  includes any pair of items that is almost linearly dependent to each other, the corresponding volume would be nearly zero, making  $A$  unlikely to be selected. De-emphasizing such cases, the DPP-based sampling serves as a subset recommender that identifies diverse items. In this study, we set the batch size  $k$  to be constant as  $k = 10$  using  $k$ -DPP [43] as follows:

$$\mathbb{P}(X = \mathcal{B}) = \frac{\det(L_{\mathcal{B}})}{\sum_{|\mathcal{B}'|=k} \det(L_{\mathcal{B}'}),} \quad (14)$$

where  $[\cdot]_{\mathcal{B}}$  denotes a submatrix indexed by the items that constitute a batch  $\mathcal{B} \in \mathcal{V}$ .

### 3.3.2 Conditional DPP

Our data collection involves recursive update of diversity kernels w.r.t. a sequence of batches. This is necessary to (*i*) avoid drawing duplicate samples that have been already observed, and to (*ii*) promote samples that are diverse not only within a given batch, but *across* a sequence of batches. DPPs are closed under conditioning operation; *i.e.* a conditional DPP is also DPP [44, 45, 46]. Let  $\mathcal{B}$  and  $\mathcal{V}$  be the batch and the ground set at the  $i$ -th iteration, respectively. Given the DPP kernel  $L^{(i)}$  at that iteration, a recursive formula for the conditional kernel  $L^{(i+1)}$  reads:

$$L^{(i+1)} = ((L^{(i)} + I_{\bar{\mathcal{B}}})_{\bar{\mathcal{B}}}^{-1})^{-1} - I, \quad (15)$$

where  $\bar{\mathcal{B}} = \mathcal{V} \setminus \mathcal{B}$ . Due to the cascaded matrix inversions – not once, but twice – involving cubic time complexity, the equation does not scale well to large-scale kernels ( $\sim O(10^4)$ ). Furthermore, t-METASET demands at least a few hundreds of conditioning. Even just *storing* (quadratic time complexity) a 88,180-size similarity kernel for  $\mathcal{D}_{TO}$  with double precision takes up about 62 gigabytes. In short, Eq. 15, as is, is intractable for large-scale similarity kernels.

### 3.3.3 Low-Rank Kernel Approximation

To circumvent the scalability issue, we leverage low-rank approximation of large-scale kernels [47]. Recalling that we have employed the Gaussian similarity kernel (Section 3.3.1), we harness the shift-invariance (*i.e.*  $L(x, y) = L(x - y)$ ) by implementing random Fourier feature (RFF) [47] as an approximation method. It grounds on the Bochner theorem [48], which guarantees that the Fourier transform  $\mathcal{F}$  of a properly scaled shift-invariant (*i.e.* stationary) kernel  $L$  is a probability measure  $\mathbb{P}(f)$  as follows:

$$L(x, y) = L(x - y) = \int_{\mathbb{R}^d} \mathbb{P}(f) \exp(jf'(x - y)) df, \quad (16)$$

where  $j$  is the imaginary unit  $\sqrt{-1}$ , and  $\mathbb{P}(f) = \mathcal{F}(L(x - y))$  is the probability distribution. With setting  $\zeta_f(x) = \exp(jf'x)$ , we recognize  $L(x, y) = \mathbb{E}_f[\zeta_f(x)\zeta_f(y)^*]$ , implying that  $\zeta_f(x)\zeta_f(y)^*$  is an *unbiased estimate* of the kernel to be approximated. The estimate variance is lowered by concatenating  $D_V$  ( $\ll n$ ) realizations of  $\zeta_f(x)$ . For a real-valued Gaussian kernel  $L$ , (*i*) the probability distribution  $\mathbb{P}(f)$  is also Gaussian and (*ii*)  $\zeta_f(x)$  reduces to cosine. Under all the considerations so far, the  $D_V \times n$  low-rank feature reads:

$$V(x) = \sqrt{\frac{2}{D_V}} [\cos(f'_1 x + b_1), \dots, \cos(f'_{D_V} x + b_{D_V})]^T, \quad (17)$$

where  $\{f_1, f_2, \dots, f_{D_V}\} \stackrel{iid}{\sim} \mathcal{N}(0, 1^2)$  and  $\{b_1, b_2, \dots, b_{D_V}\} \stackrel{iid}{\sim} \mathcal{U}[0, 2\pi]$ . The low-rank feature update  $V'$  conditioned on  $\mathcal{B}$  has the following closed-form expression [46]:

$$V' = V_{\bar{\mathcal{B}}} Z^{\mathcal{B}} (I - V_{\mathcal{B}}^T (V_{\mathcal{B}} V_{\mathcal{B}}^T)^{-1} V_{\mathcal{B}}), \quad (18)$$

where the true kernel is  $L \approx V'(V')^T$ . Now the matrix inversions become amenable as the time complexity decreases to  $O(|\mathcal{B}|^3)$  with  $|\mathcal{B}| = k \ll n$ .

### 3.3.4 Quality-Weighted Diversity for Task-Aware Sampling

Lastly, we take into account user-defined quality, in addition to diversity, to construct datasets that are not only balanced but also *task-aware*. This study is dedicated to *pointwise* design quality, where a pointwise  $n \times 1$  quality vector  $q(z, \hat{p})$  associated with a design task serves as an additional weight to the low-rank feature  $V$ . The resulting feature  $D_v \times n$  matrix  $V''$  reads

$$V'' = \overbrace{[q(z, \hat{p}^{(t)}) \dots q(z, \hat{p}^{(t)})]}^{D_v} [T] \circ V', \quad (19)$$

where  $\circ$  denotes the Hadamard product (*i.e.* elementwise multiplication).

The quality-weighted DPP sampling seems to have an analogy with Bayesian optimization (BO) [39] in that: (*i*) quality contributes to exploitation given design attributes of interest, whereas diversity does to exploration, and (*ii*) both use sequential sampling. We highlight the differences as well: (*i*) diversity is still the main driver of the sequential DPP sampling, whereas in BO exploration (diversity) is ultimately a means for exploitation (quality); (*ii*) t-METASET handles quality that accommodates distributional attributes of shape, property, and even the combination of them, while for BO property distributions could be difficult to control; (*iii*) t-METASET has more flexibility in terms of tailoring distributional characteristics, while standard BO ends up biasing both shape and property distributions to reach the global optimum of a black-box cost function; (*iv*) t-METASET is primarily driven by *pairwise* DPP kernels, taking a pointwise quality as an optional “ad-hoc”, whereas BO is driven by a *pointwise* acquisition function, and (*v*) t-METASET does not take the uncertainty provided by the GP regressor – at least under the current setup – as a sampling criterion. Quantitative validation of t-METASET against BO would be interesting topic yet is currently infeasible, as t-METASET can only downsample out of  $|\mathcal{S}|$  *finite* points in the VAE latent space, whereas standard BO takes *infinitely many* continuous inputs. Yet, the validation could be viable under the following extensions: (*i*) the decoder of the VAE joins as part of the t-METASET to generate new shapes  $\hat{\phi}(x, y) = G(z)$  beyond the existing shapes in  $\mathcal{S}$ , and (*ii*) t-METASET extends to continuous DPP [49] to recommend diverse samples from an approximated *continuous* distribution, beyond the discrete datapoints provided by users. This is our future work.

## 3.4 The t-METASET Algorithm

In this section, we detail how to seamlessly integrate the three main components introduced: (*i*) the latent shape descriptor from the shape VAE, (*ii*) a sparse regressor as the start-up agent, and (*iii*) the batch sequential DPP-based sampling that suppresses undesirable bias and enforces desirable one. Visual illustration of t-METASET is presented in Figure 4.

### 3.4.1 Initialization

Figure 4(b) illustrates the initialization of t-METASET, which involves VAE training, shape descriptor, and RFF-based low-rank feature extraction of the latent shape descriptor based on the shape-only data sets. The t-METASET takes the following input arguments: the shape-only dataset  $\mathcal{S}$  comprising SDF instances  $\phi(x, y) \in \mathcal{S}$  (also applicable to pixel/voxel images or point clouds [34, 10]), batch cardinality  $k$ , the ratio of property samples in each batch  $\epsilon$ , and optionally a pointwise quality function  $q(z, \hat{p})$  that reflects a design task declared in advance. A shape VAE is trained on  $\mathcal{S}$  with the dimension of latent space  $D_z$  as 10-D (Figure 4(b)). Then we draw  $D_v \times n$  low-rank RFF  $V_z$  (17) of the  $n \times n$  shape similarity kernel  $L_z$ . In this study, we set the low-rank feature size as  $D_v = 3,000$ . This feature is to be recursively updated based on conditioning on a series of batches to be collected. For initialization of conditional DPPs given the shape feature, we follow the procedure of R.H. Affandi *et al.* [45].

### 3.4.2 Stage I

During Stage I, the roughness shows large fluctuation due to lack of data. The sampling only relies on shape diversity, because the property prediction of the GP given unseen latent variables is not reliable yet. This stage also can be viewed as initial exploration driven by the pairwise shape dissimilarity – as an analog to initial passive space-filling design – under  $|\mathcal{D}| \sim O(10^4)$  discrete datapoints.

### 3.4.3 Stage II

Figure 4(c) provides an overview of Stage II – the core sampling stage of t-METASET. As more data come in, the roughness residual  $r^{(t)}$  (Eq. 10) approaches to zero and becomes stable. Provided that the roughness residual falls under the first threshold  $\tau_1$  for five consecutive iterations, the t-METASET framework assumes that the GP prediction is ready to be appreciated. t-METASET transits to the next sampling phase Stage II, where t-METASET uses *estimated* property

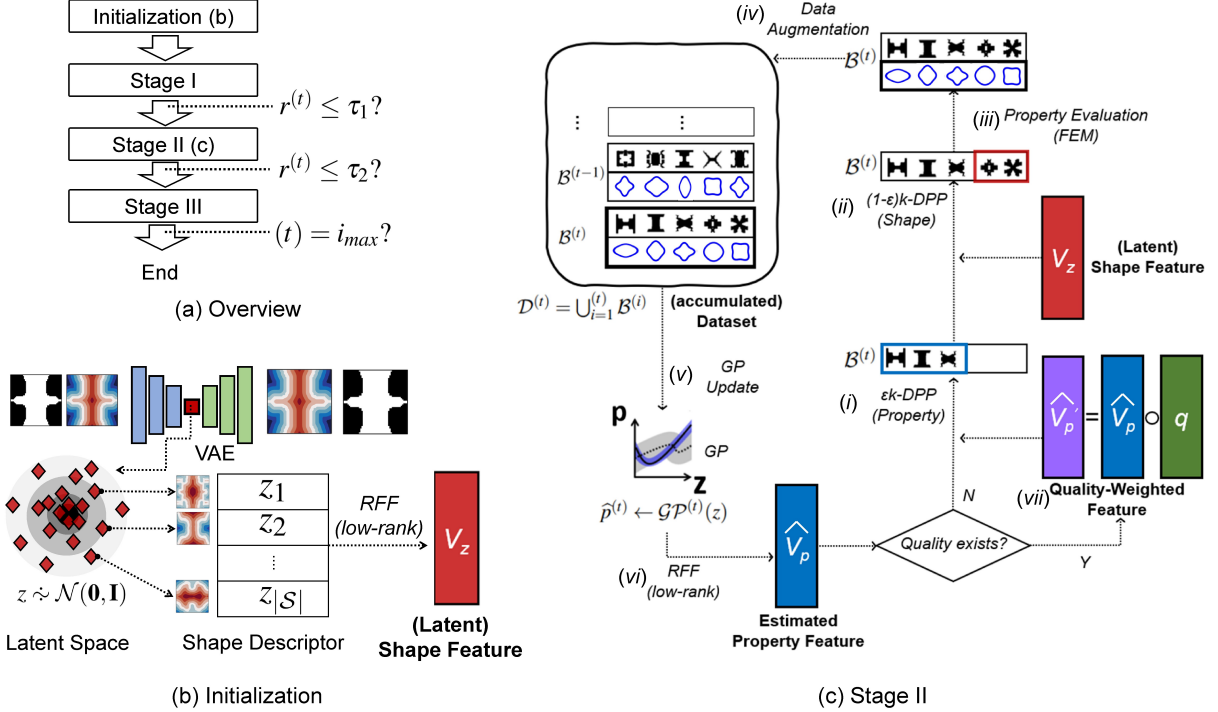


Figure 4: Visual illustration of t-METASET. (a) Overview. (b) Initialization. The VAE is trained on the given shape-only dataset  $\mathcal{S}$ . The latent variables are roughly distributed as multivariate Gaussian. The latent representation is taken as the shape descriptor, whose concatenation forms the  $|\mathcal{S}| \times D_z$  matrix, where  $|\mathcal{S}|$  is the shape set cardinality ( $\sim O(10^4)$ ). RFF follows to obtain a  $|\mathcal{S}| \times D_v$  low-rank feature of shape feature to be used for the DPP sampling based on shape diversity. (c) A simplified flowchart of Stage II. Details of are stated in the main body. Stage I shares the structure of Stage II but is driven only by shape feature. Stage III is equivalent Stage II except GP update.

diversity, in addition to shape diversity, as the main criterion. The key is to introduce the low-rank *estimated* property RFF  $\hat{V}_p$  building on the GP prediction  $\hat{p} = \mathcal{G}(z)$ .

Now we walk you through each step described in Figure 4(c). (i) Given a batch composition  $\epsilon$ , the DPP sampler draws  $\epsilon k$  (integer) instances from the property RFF to control property distribution. (ii) The rest of the batch is filled by  $(1 - \epsilon)k$  samples from the shape RFF, to complement potential lack of exploration in the shape descriptor space  $\Omega_z$ . Herein, the shape RFF must be updated with respect to batch  $\mathcal{B}_\epsilon$  first, to reflect the latest information. Once sampled, the shape feature is updated again with respect to the rest shapes in  $\mathcal{B}_{1-\epsilon}$  just selected, for the next iteration. (iii) The microstructures of the batch are observed by design evaluation – FEM with energy-based homogenization [50, 51] in this study – to obtain the true properties (e.g.,  $p = \{C_{11}, C_{12}, C_{22}\}$ ). (iv) The true properties replace the GP prediction in the given batch  $\mathcal{B}^{(t)}$ . (v) Then the evaluated batch updates the GP to refine the property prediction as  $\hat{p}^{(t)} = \mathcal{G}\mathcal{P}^{(t)}(z)$  for the next iteration. (vi) The refined prediction demands the update of a new property RFF, and to condition it on the whole data  $\mathcal{D}^{(t)} = \bigcup_{i=1}^t \mathcal{B}^{(i)}$  collected by then. (vii) If a quality function  $q(z, \hat{p})$  over design attributes has been specified, it can be incorporated into the latest property RFF by invoking Eq. 19, to prompt a “task-aware” dataset.

### 3.4.4 Stage III

Stage III shares all the settings of Stage II except for the GP update. The main computational overhead of Stage II comes from GP fitting as it involves matrix inversion with the time complexity  $\sim O(|\mathcal{D}^{(t)}|^3)$ . To bypass the overhead, we stop updating the GP if the roughness residual falls under  $\tau_2 = 0.01$  for five consecutive iterations. During Stage III, our algorithm can quickly identify diverse instances from a large-scale dataset ( $\sim O(10^4)$ ), without scalability issue. The main product of t-METASET is a high-quality dataset  $\mathcal{D} = \bigcup_{i=1}^{i_{max}} \mathcal{B}^{(t)}$ , which is not only diverse but task-aware. In this study, we particularly focus on producing datasets with size of either 3,000 or 5,000.

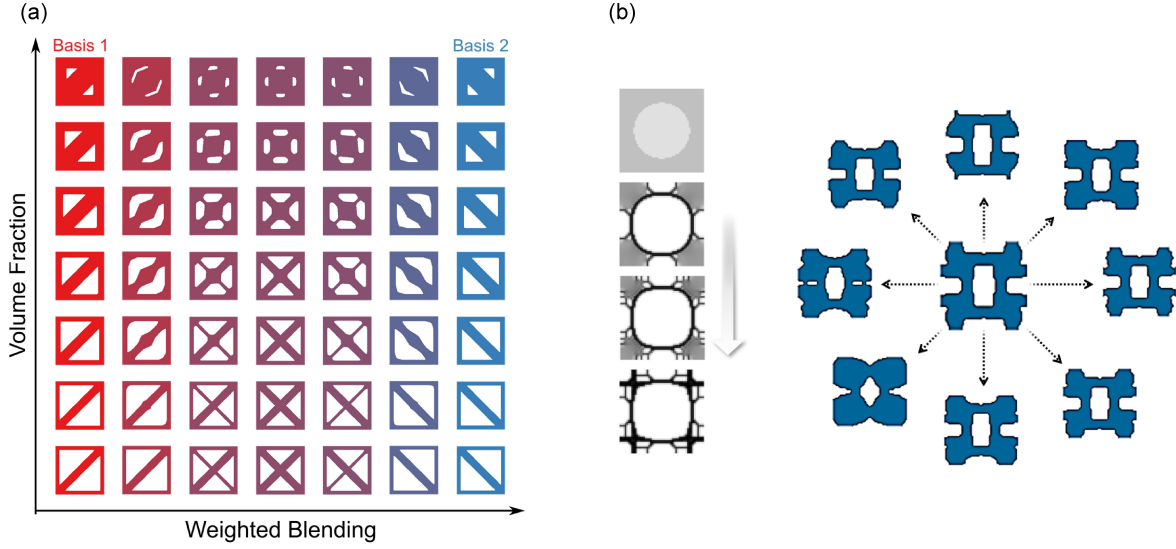


Figure 5: Illustration on shape generation schemes of each dataset. (a)  $\mathcal{D}_{mix}$  [19]: example of blending the SDFs of basis shapes and varying their volume fractions to produce new unit cells. (b)  $\mathcal{D}_{TO}$  [32]: (left) an example of design evolution by inverse topology optimization w.r.t. a target property; (right) stochastic shape perturbation applied to a given microstructure.

## 4 Results

In this section, the results of t-METASET are presented. As benchmarks, the two large-scale mechanical metamaterial libraries are used for the validation [19, 32]. Data description on the two datasets is provided in Section 4.1. We propose an interpretable diversity metric in Section 4.2 for fair evaluation of t-METASET. To accommodate various end-uses in DDMD, we validate t-METASET under three hypothetical deployment scenarios: (i) *diversity only* for generic use (balanced datasets; Section 4.3), (ii) *quality-weighted diversity* for particular use (task-aware datasets; Section 4.4), and (iii) *joint diversity* for tailororable use (tunable datasets; Section 4.5).

### 4.1 Datasets

We introduce two mechanical metamaterial datasets, in addition to  $\mathcal{D}_{lat}$ , to be used for validating t-METASET: (i) 2-D multiclass blending dataset ( $\mathcal{D}_{mix}$ ) [19], and (ii) 2-D topology optimization dataset ( $\mathcal{D}_{TO}$ ) [32]. Table 1 compares key characteristics of the datasets. Figure 5 illustrates each dataset and their shape generation heuristic. Note that the purpose of involving the two datasets is to corroborate the versatility of our t-METASET framework in that the method can accommodate a wide range of datasets, born from different methods for different end-uses, in a unified and principled way. What we aim to provide is quality assessment *within* one of the datasets, *not across* them. In addition, while all the datasets in the original references provide the homogenized properties, we assume in all the upcoming numerical experiments that only the shapes are given, *without any property evaluated a priori*.

### 4.2 Diversity Metric: Distance Gain

We discuss an interpretable diversity metric needed to quantitatively evaluate the efficiency of t-METASET. In the literature of DDMD, Y. C. Chan *et al.* [11] compared the determinant of jointly diverse subsets' similarity kernels against those of *iid* replicates, following the usual practice of reporting set diversity in the DPP literature [18], as the metric to claim the efficacy of the proposed downsampling. We point out possible issues of using either similarity or determinant for diversity evaluation: (i) similarity values  $s_{ij}$  depend on data preprocessing; (ii) a decreasing transformation from distance to similarity ( $s_{ij} = T(h(x_i, x_j))$ ) for constructing DPP kernels also involves arbitrary scaling, depending on the type of associated transformation  $T$  and their tuning parameters (e.g., bandwidth of the Gaussian kernels); (iii) the raw values of both similarity and determinant enable the “better or worse” type comparison yet lack intuitive interpretation on “*how much better or worse*”.

Table 1: Dataset Description

	$\mathcal{D}_{lat}$ [15]	$\mathcal{D}_{mix}$ [19]	$\mathcal{D}_{TO}$ [32]
Cardinality	9,882	57,000	88,180
Shape primitive	Bar	SDF of basis unit cell	N/A (used TO)
Shape population	Parametric sweep	Continuous sampling of basis weights & Blending	Stochastic shape perturbation & Iterative sampling
Topological freedom	Predefined	Quasi-free	Free
Property	$\{C_{11}, C_{12}, C_{22}, C_{13}, C_{23}, C_{33}\}$	$\{C_{11}, C_{12}, C_{22}\}$	$\{C_{11}, C_{12}, C_{22}\}$
FEM discretization	$100 \times 100$	$50 \times 50$	$50 \times 50$
FEM solver		Energy-based homogenization [50, 51]	

To this end, we propose a distance-based metric that is more interpretable and less arbitrary. Given a metamaterial set  $\mathcal{D}$ , we compute the mean Euclidean distance  $\bar{d}$  of pairwise distances of attributes (shape/property) as

$$\bar{d}(\mathcal{D}) = \frac{1}{|\mathcal{D}|} \sum_{j=1}^{|\mathcal{D}|} \sum_{i=1}^{|\mathcal{D}|} h(x_i, y_j) = \frac{1}{|\mathcal{D}|} \sum_{j=1}^{|\mathcal{D}|} \sum_{i=1}^{|\mathcal{D}|} \sqrt{\|x_i - x_j\|^2}. \quad (20)$$

Intuitively, the larger  $\bar{d}(\mathcal{D})$  is, the more diverse  $\mathcal{D}$  is. The mean metric still depends on data preprocessing, as similarity does. Herein, key idea is to normalize  $\bar{d}(\mathcal{D})$  it with that of an *iid* counterpart  $\bar{d}(\mathcal{D}_{iid})$  with the same cardinality  $|\mathcal{D}_{iid}| = |\mathcal{D}|$  so that data preprocessing does not affect in a relative sense. To account for the stochasticity of *iid* realizations, we generate  $n_{rep} = 30$  replicates, take the mean of each mean distance, and compute the relative *gain*  $h_G$  as:

$$h_G = \frac{\bar{d}(\mathcal{D})}{\frac{1}{n_{rep}} \sum_{l=1}^{n_{rep}} \bar{d}((\mathcal{D}_{iid})_l)}, \quad (21)$$

where  $(\mathcal{D}_{iid})_l$  denotes the  $l$ -th *iid* replicate with  $|(\mathcal{D}_{iid})_l| = |\mathcal{D}|$ . We call the diversity metric “distance gain”, as the metric *relatively* gauges how more diverse a given set is compared to *iid*. For example, the gain of 1.5 given a property set  $\mathcal{P}$  implies that the Euclidean distances between property pairs are 1.5 times larger on average than those of  $\mathcal{P}_{iid}$  in the property space. The proposed metric offers intuitive interpretation based on distance, avoids the dependency on both data scaling and distance-to-similarity transformation, and thus offers a means for fair diversity evaluation of a given dataset. In addition, the metric generalizes to sequential sampling with  $h_G^{(t)}$  at  $t$ -th iteration as well, allowing quantitative assessment across iterations involving different cardinality. Hence, we report all the upcoming results based on the distance gain proposed.

### 4.3 Scenario I: Diversity Only

Figure 6 shows the t-METASET results applied to  $D_{TO}$  only based on diversity. The basic setting includes: batch cardinality as  $k = 10$ ; property sample ratio during Stage II as  $\epsilon = 0.8$ , maximum iteration as  $i_{max} = 500$ ; first and second threshold of roughness parameters as  $\tau_2 = 0.02$  and  $\tau_1 = 0.01$ , respectively; iteration tolerance of roughness convergence as  $i_{tol} = 5$ ; the number of *iid* replicates for distance gain as  $n_{rep} = 30$ .

From Figure 6(a), we observe the evolution of the distance gain, as a relative proxy for set diversity, at each iteration. At Stage I the proposed sampling solely relies on shape diversity. The shape gain exceeds unity at the early stage, meaning the exploration by t-METASET shows better shape diversity than that of the *iid* replicates. Meanwhile, property diversity of t-METASET is even less than the *iid* counterpart; this is another evidence that shape diversity does not necessarily contribute to property diversity [11]. During this transient stage, t-METASET keeps monitoring the residual of roughness parameters. Figure 6(b) shows the history up to few hundred cardinality; the residuals with little data show large residuals, indicating large fluctuations of the hyperparameters. The mild convergence defined by  $\tau_1$  occurs at the 19-th iteration with  $10 \times 19 = 190$  observations. This is approximately twice larger than the rule-of-thumb for the initial space-filling design:  $D_z \times 10 = 100$  [52]. Rigorous comparison between our pairwise based initial exploration and space-filling design (e.g., Latin hypercube sampling [53]) is future work.

Once the first convergence criterion on the GP roughness  $\omega$  is met, t-METASET starts to respect the GP prediction and, by extension, the low-rank feature of the estimated property DPP kernel as well. During Stage II, shape diversity decreases less than unity. This implies that pursuing property diversity causes a compromise of shape diversity. After about 300 iterations, each gain seems to stabilize with minute fluctuations, and reach a plateau of about 1.3 for

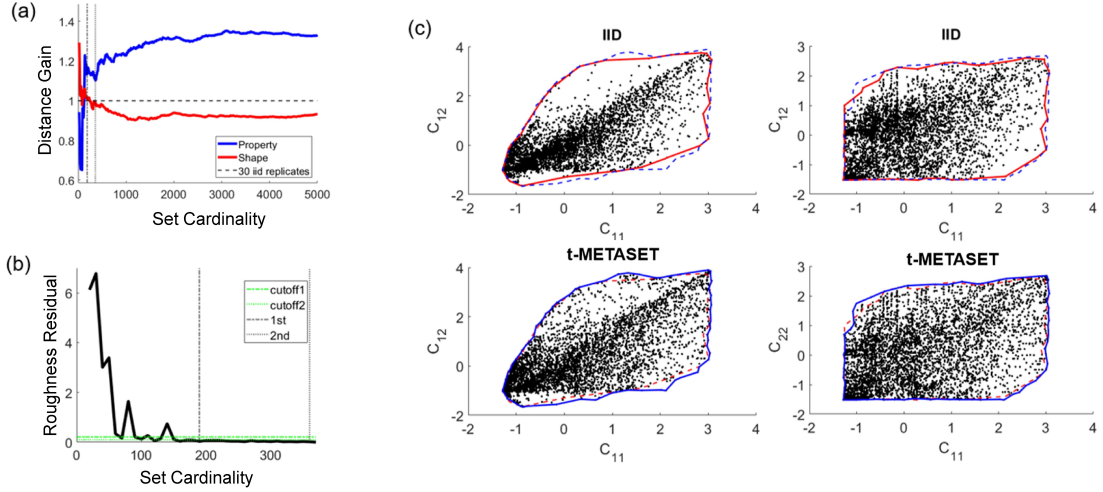


Figure 6: Scenario I result for  $\mathcal{D}_{TO}$ . (a) History of distance gains. The horizontal dotted line denotes the distance gain of 30 iid replicates, which is unity by the definition in Section 4.2. The two vertical lines indicate the first ( $\tau_1$ ) and second ( $\tau_2$ ) roughness convergence, respectively. (b) History of roughness residual. The two vertical lines indicate the first and second roughness convergence, respectively. (c) Property distribution in projected property space

property and 0.95 for shape, respectively. Beyond the maximum iteration set as 500, we forecast that the mean of property Euclidean distances – the numerator of property gain – will eventually decrease because: (i) we have finite  $|\mathcal{D}_{TO}| = 88,180$  shapes to sample from; (ii) the property gamut  $\partial\Omega_p^{(t)}$  at the  $t$ -th iteration grows yet ultimately approaches to the finite gamut as  $\partial\Omega_p^{(t)} \rightarrow \partial\Omega_p^*$ , where  $\partial\Omega_p^*$  denotes the property gamut of fully observed  $\mathcal{D}_{mix}$ , which obviously exists yet is unknown in our scenarios; (iii) adding more datapoints within the confined boundary  $\partial\Omega^*$  would decrease pairwise distances on average. The convergence behavior of the numerator of the property gain may possibly give a hint to answering the fundamental research question in data-driven design: “*How much data do we need?*”. This is our future work. In addition, adjusting the batch composition – the ratio of property versus shape – would lead to different results. The parameter study on  $\epsilon$  is addressed and discussed in Section 4.5.

Figure 6(c) shows a qualitative view on the resulting property distributions. Figure 6(c) shows data distribution in the projected property space, whose property components have been standardized. In the  $C_{11}$ - $C_{12}$  space, the iid realization shows significant bias on the southeast region near  $[-1 \leq C_{11} \leq 1] \times [-1.5 \leq C_{12} \leq 1]$ , whereas only tiny samples are located on the upper region. Other 3,000-size iid realizations also result in property bias: local details are different, but the overall distributional bias is more or less the same. On the other hand, the property distribution of t-METASET shows significantly reduced bias in the property spaces, in terms of projected pairwise distances and the property gamut  $\partial\Omega_p$  as well.

#### 4.4 Scenario II: Task-Aware Quality-Weighted Diversity

Diversity alone does not ensure successful deployment of DDMD for design purposes. Imagine a case where a 50k-size dataset with perfect uniformity has been prepared, yet the region of design interest happens to include few samples. In such a scenario, *artificial data bias is rather desirable* to invest more resources in the region of central interest, which can be declared by users. The scope of this work is dedicated to *pointwise* quality, where the task-related “value” of each observation is modeled based on a score function. It can be a function of properties (e.g., stiffness anisotropy), shape (e.g., boundary smoothness), or even both (stiffness-to-mass ratio). With a proper formulation and scaling, the quality function can join t-METASET as a secondary supervisor. We present two examples, each of which involves either (i) only property (Section 4.4.1) or (ii) both shape and property (Section 4.4.2), respectively. All the results in this subsection assumes the maximum cardinality is fixed as  $|\bigcup_{l=1}^{i_{max}} \mathcal{B}^{(l)}| = 3,000$ .

##### 4.4.1 Task II-1: Stiffness-to-Mass Ratio

Oustanding stiffness-to-mass ratio is one of the key advantages of mechanical metamaterial systems against conventional structures [1]. If lightweight design is of interest, users could attempt to prioritize observations with high stiffness-to-

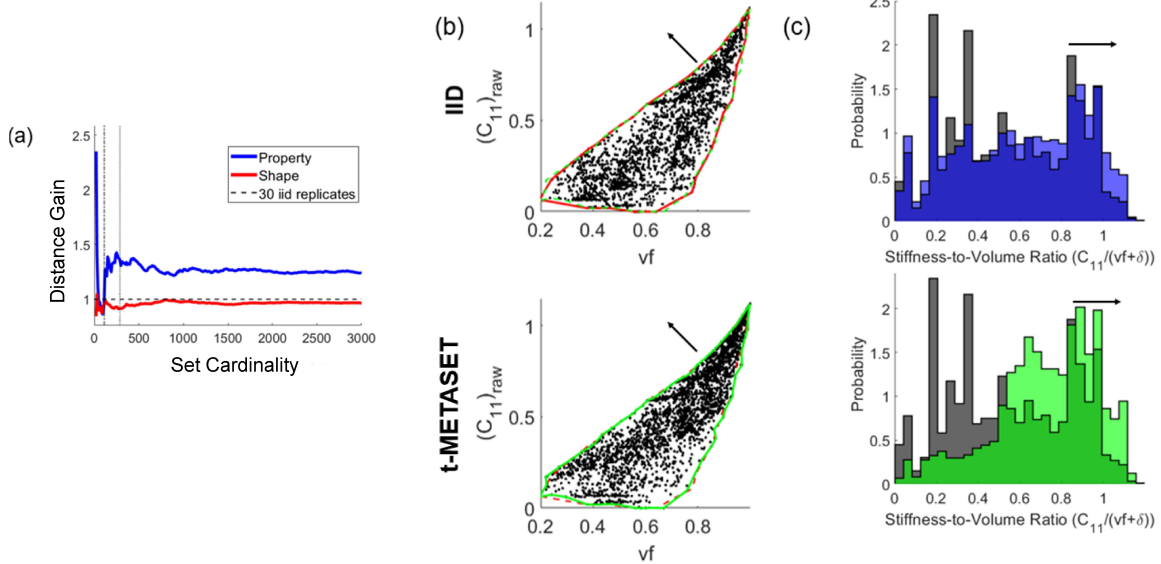


Figure 7: Task II-1 (stiffness-to-mass ratio) result for  $\mathcal{D}_{mix}$ . Each black arrow indicates the preferred direction of distributional bias. (a) History of distance gains. (b) Data distribution in the attribute space of interest. (c) Histogram of the quality metric: (top) *iid* (gray) vs t-METASET (blue); (bottom) *iid* (gray) vs t-METASET with  $q_1$  (green).

mass ratio. We take  $C_{11}$  as an example to with an associated score  $q(\cdot)$  formulated as

$$q_1(z, \hat{p}) = \frac{\widehat{C}_{11}}{v_f + \delta} \quad (22)$$

where  $v_f$  is the volume fraction of a given binary shape  $I(x, y)$  implicitly associated with  $z$ , and  $\delta$  is a small positive number to avoid singularity. Here, we use raw values of  $C_{11}$  to ensure that all the values are nonnegative. Note that the property  $\hat{p}$  takes both (i) ground-truth properties from the finite element analysis and (ii) predicted properties from the regressor  $\mathcal{GP}$ . To accommodate various datasets at different scales without manual scaling, we standardize  $q_1$  into  $q'_1$ . Then it is passed to the following sigmoid transformation:  $a_1(\cdot) = 1 - 1/(1 + \exp(-20(\cdot)))$ , where  $a_1(\cdot)$  is the decreasing sigmoid activation. To accommodate the design attributes associated with the quality function  $a_1(q')$ , the low-rank feature  $V$  of the property diversity kernel  $\widehat{L}_P$  has the pointwise quality on board according to Eq. 19.

Figure 7 presents the result for  $\mathcal{D}_{mix}$ . As indicated by the arrow, the quality function aims to bias the distribution in the  $(C_{11})_{\text{raw}}-v_f$  space towards the northwest direction. For  $C_{11}$ , we used its raw value for better scaling with volume fraction  $v_f$ . In Figure 7(b), the resulting distribution of t-METASET shows an even stronger bias to the upper region than that of the *iid* replicates, whereas the datapoints near the bottom right gamut are more sparse. Figure 7(c) provides even more intuitive evidence: (top) t-METASET without the quality function does not show distributional difference with the *iid* case. (bottom) In contrast, the quality-based t-METASET leads to the strongly biased distribution – virtually opposite to the *iid* one – congruent with the enforced quality over high stiffness-to-volume ratio. Both plots corroborate that t-METASET can accommodate the preference of high stiffness-to-volume ratio, *even when starting with no property at all*. Along the way, t-METASET addresses property diversity as well, as indicated by the distance gain of property that exceeds unity (Figure 7(a)).

#### 4.4.2 Task II-2: Stiffness Anisotropy

Property anisotropy of unit cells is another key quality that mechanical metamaterials could leverage to achieve strong directional performances at system levels. With  $\mathcal{S}_{TO}$ , we attempt to deliberately bias the property distribution towards strong elastic anisotropy between  $C_{11}$  and  $C_{22}$ . We devise the anisotropy index as the associated quality function:

$$q_2(z, \hat{p}) = \frac{|\arctan(\widehat{C}_{22}/\widehat{C}_{11}) - \pi/4|}{\pi/4}, \quad (23)$$

where  $\widehat{C}_{11}$  and  $\widehat{C}_{22}$  denote the raw non-negative elastic constants predicted by the GP model, without any normalization;  $\arctan(\widehat{C}_{22}/\widehat{C}_{11}) \in [0, \pi/2]$  is the polar angle in the  $C_{11}$ - $C_{22}$  space. If isotropic (*i.e.*  $C_{11} = C_{22}$ ), the index is 0. As

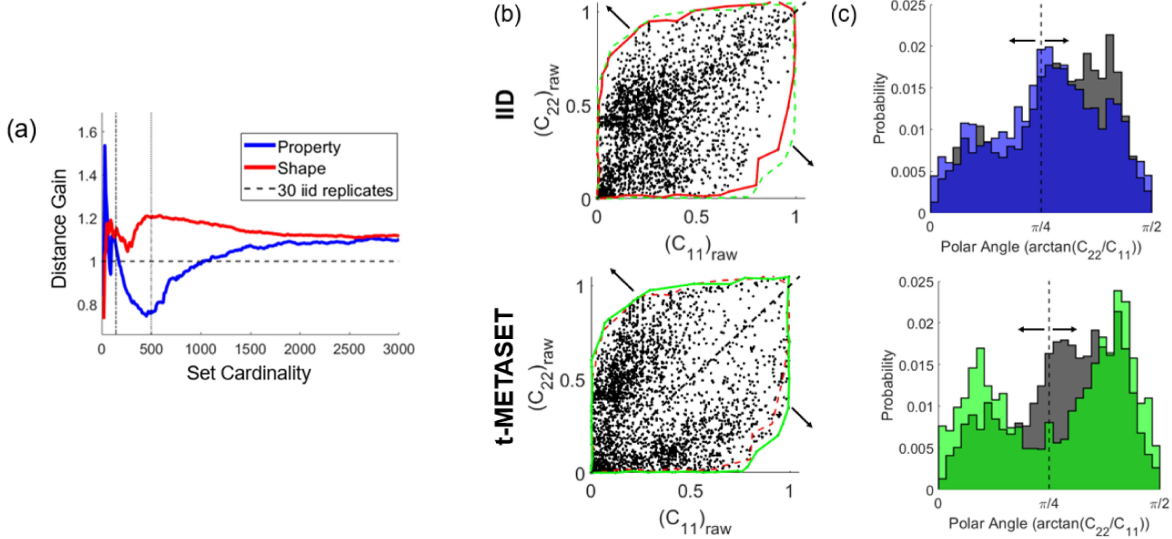


Figure 8: Task II-2 (stiffness anisotropy) result for  $\mathcal{D}_{TO}$ . Each black arrow indicates the preferred direction of distributional bias. (a) History of distance gains. (b) Data distribution in the attribute space of interest. (c) Histogram of polar angles of data: (top) *iid* (gray) vs t-METASET (blue); (bottom) *iid* (gray) vs t-METASET with  $q_2$  (green).

either  $C_{22}/C_{11} \rightarrow 0^+$  or  $C_{22}/C_{11} \rightarrow \infty$ , the index goes to 1. By the definition the quality function ranges between  $[0, 1]$ . We directly pass it to a monotonically increasing sigmoid activation:  $a_2(\cdot) = 1/(1 + \exp(-20((\cdot) - 0.5)))$ . In a similar vein with the first example above,  $a_2(q_2)$  is incorporated to the low-rank property feature using Eq. 19.

Figure 8 illustrates the result for  $\mathcal{D}_{TO}$  under the anisotropy preference. The two arrows indicate the bias direction of interest: Samples with isotropic elasticity on the line  $C_{22} = C_{11}$ , denoted as the black dotted line, are least preferred. From the scatter plot of Figure 8(a), the distribution of t-METASET exhibits clear bias towards the preferred direction, compared to the *iid* case, while samples near the isotropic line is sparse except near the origin. The trend is even more apparent in the histograms of Figure 8(b): both the results from *iid* and vanilla t-METASET share a similar distribution in terms of polar angle. In contrast, task-aware t-METASET exhibits a bimodal distribution that is highly skewed to either 0 and  $\pi/2$ .

In Figure 8(a), we recognize an interesting point that reveals the power of t-METASET: unlike the other cases introduced, the shape gain also exceeds unity at the plateau stage, with a mild loss in the property gain. Note that we did *not* enforce the framework to assign more resources on shape diversity; (i) the quality function  $q_2(C_{11}, C_{22})$  has been defined over only the two properties, *not* shape, and (ii) during Stage II t-METASET can take only two samples from shape diversity in each batch due to the setting  $\epsilon = 0.8$ , commonly shared by the other cases introduced. This indicates that: the decent exploration in the shape space – the shape gain even large than the property gain during Stage II – is *what t-METASET autonomously decided on its own via active learning, to fulfill the mission specified by the given task*. The result demonstrates the power of t-METASET in that, given a large-scale dataset and on-demand design quality, it can *intelligently* decide how to properly tailor distributional biases in shape/property space to meet given design goals, without human supervision.

We emphasize that the result came out from the same algorithmic settings of t-METASET shared with the other cases, except for the quality functions. Hence, the two case studies, investigated with respect to different datasets and different quality functions, demonstrate that t-METASET has fulfilled the mission: growing task-aware yet balanced datasets by active learning.

#### 4.5 Scenario III: Joint Diversity

The proposed t-METASET can tune joint diversity when building datasets. Y. C. Chan *et al.* [11] demonstrated that, given a *fully observed* dataset, the DPP-based sampling method can identify a representative subset with adjustable joint diversity [11]. The capacity builds on the fact that any linear combination of PSD shape/property kernels to create the joint diversity  $L_J = (1 - \epsilon)L_s + \epsilon L_p$  is also PSD. Yet the linear combination approach does not apply to our proposed

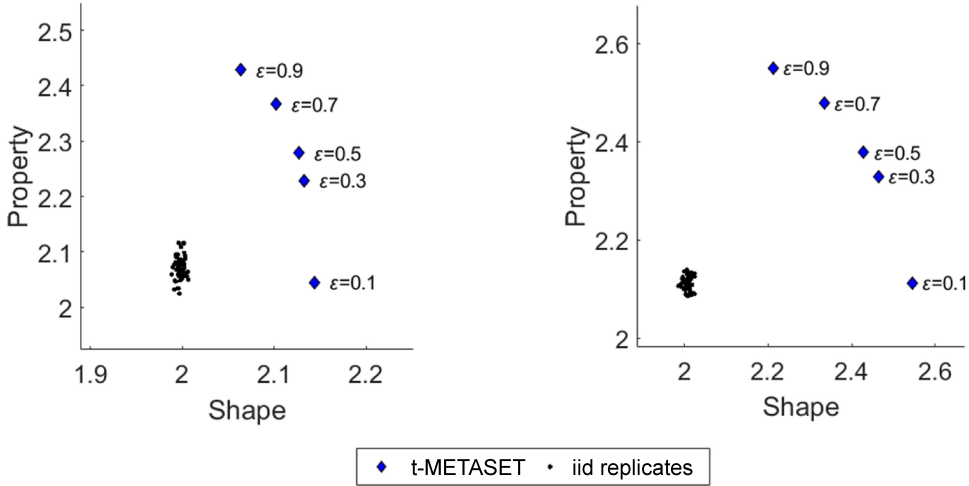


Figure 9: Scenario III (joint diversity) results for  $\mathcal{D}_{mix}$  and  $\mathcal{D}_{TO}$ .  $\epsilon$  denotes the ratio of property samples in each batch. (a) Mean Euclidean distance for  $\mathcal{D}_{mix}$ . (b) Mean Euclidean distance for  $\mathcal{D}_{TO}$ .

t-METASET, driven by the low-rank feature  $V$ , because the linear combination of  $V$  does not guarantee the resulting joint kernel to be PSD.

Instead, our framework achieves joint diversity by adjusting the shape/property sampling ratio  $\epsilon$  of a batch. Figure 9 shows the parameter study over the batch composition  $\epsilon$  with respect to  $\mathcal{D}_{mix}$  and  $\mathcal{D}_{TO}$  with  $|\bigcup_{l=1}^{l_{max}} \mathcal{B}^{(l)}| = 5,000$ . Both results manifest (i) better average diversity in terms of Euclidean distances than that of the *iid* replicates, and (ii) the trade-off between shape diversity and property diversity. Additionally, the results support the previous finding: the near-zero correlation between shape diversity and property diversity [11]. The substantial distinction of t-METASET lies in: We *sequentially* achieve the jointly diverse datasets, *beginning from scratch in terms of property*. In addition, t-METASET can dynamically adjust  $\epsilon$  as well, based on either manual real-time monitoring over diversity gains or some user-defined rigorous criteria. This capacity could possibly help designers steer the sequential data acquisition at will, in particular if growing a large-scale dataset ( $\sim O(10^4)$ ) is of interest, where applying a single sampling criterion over the whole generation procedure might not necessarily result in the best dataset for given design tasks.

## 5 Conclusion

We have presented the task-aware METASET (t-METASET) framework dedicated to task-aware acquisition of metamaterial datasets. Uniquely, t-METASET specializes in a scenario that designers often encounter in early stages of DDMD: a massive shape library has been prepared with no properties observed for a new design scenario. The central idea of t-METASET for building a task-aware dataset, in general, is to (i) leverage a compact yet expressive shape descriptor (VAE latent representation) for shape dimension reduction, (ii) sequentially update a sparse agent model (e.g., GP) for the nonlinear regression with sparse observations, and (iii) sequentially sample in the shape descriptor space based on estimated property diversity and estimated quality (DPP) for distribution control of shape/property. t-METASET contributes to the design research by: (i) proposing a data acquisition methodology *at early stages of data collection*, (ii) *sequentially* combating *property bias*, and along the way (iii) accommodating *task-aware design quality* as well. We emphasize again that, starting without evaluated properties, all the results tested on two large-scale metamaterial datasets ( $\mathcal{D}_{mix}$  and  $\mathcal{D}_{TO}$ ) were automatically achieved by t-METASET, in three different scenarios, without human supervision and arduous parameter tuning. We argue t-METASET can handle a variety of metamaterial datasets in general, by virtue of scalability, modularity, task-aware data customizability, and independence from both shape generation heuristics and domain knowledge.

The imperative future work is inference-level validation of dataset quality, which aims to shed light on the downstream impact of data quality at deployment stage of data-driven models. Among a plethora of data-driven models, we are particularly interested in conditional generative models [54, 55], due to their on-the-fly inverse design capability expected to be highly sensitive to data quality. The validation would further demonstrate the efficacy of t-METASET at

a high level, in addition to that which we have shown at the intuitive metric level. Moreover, we point out two interesting topics to be explored: (i) the proposed diversity gain as a termination indicator of data generation, which could offer insight into “*how much data?*” (detailed in Section 4.3) and (ii) quantitative comparison between the quality-weighted diversity sampling (Section 3.3.4) presented in this work and Bayesian optimization [39].

Through producing and sharing open-source datasets, t-METASET ultimately aims to (i) provide a methodological guideline on how to generate a dataset that can meet individual needs, (ii) publicly offer datasets as a reference to a variety of benchmark design problems in different domains, and (iii) help designers diagnose their dataset quality on their own. This will lay solid foundation for the future advancements of DDMD.

## Acknowledgment

We acknowledge funding support from the National Science Foundation (NSF) through the CSSI program (Award # OAC 1835782).

## References

- [1] Xianglong Yu, Ji Zhou, Haiyi Liang, Zhengyi Jiang, and Lingling Wu. Mechanical metamaterials associated with stiffness, rigidity and compressibility: A brief review. *Progress in Materials Science*, 94:114–173, 2018.
- [2] Costas M Soukoulis and Martin Wegener. Past achievements and future challenges in the development of three-dimensional photonic metamaterials. *Nature photonics*, 5(9):523–530, 2011.
- [3] Steven A Cummer, Johan Christensen, and Andrea Alù. Controlling sound with acoustic metamaterials. *Nature Reviews Materials*, 1(3):1–13, 2016.
- [4] Robert Schittny, Muamer Kadic, Sébastien Guenneau, and Martin Wegener. Experiments on transformation thermodynamics: molding the flow of heat. *Physical review letters*, 110(19):195901, 2013.
- [5] Muamer Kadic, Tiemo Bückmann, Robert Schittny, and Martin Wegener. Metamaterials beyond electromagnetism. *Reports on Progress in physics*, 76(12):126501, 2013.
- [6] Ruopeng Liu, Chunlin Ji, Zhiya Zhao, and Tian Zhou. Metamaterials: reshape and rethink. *Engineering*, 1(2):179–184, 2015.
- [7] Bo Zhu, Mélina Skouras, Desai Chen, and Wojciech Matusik. Two-scale topology optimization with microstructures. *ACM Transactions on Graphics (TOG)*, 36(4):1, 2017.
- [8] Zhaocheng Liu, Dayu Zhu, Sean P Rodrigues, Kyu-Tae Lee, and Wenshan Cai. Generative model for the inverse design of metasurfaces. *Nano letters*, 18(10):6570–6576, 2018.
- [9] Wei Ma, Feng Cheng, Yihao Xu, Qinlong Wen, and Yongmin Liu. Probabilistic representation and inverse design of metamaterials based on a deep generative model with semi-supervised learning strategy. *Advanced Materials*, 31(35):1901111, 2019.
- [10] Liwei Wang, Yu-Chin Chan, Faez Ahmed, Zhao Liu, Ping Zhu, and Wei Chen. Deep generative modeling for mechanistic-based learning and design of metamaterial systems. *Computer Methods in Applied Mechanics and Engineering*, 372:113377, 2020.
- [11] Yu-Chin Chan, Faez Ahmed, Liwei Wang, and Wei Chen. Metaset: Exploring shape and property spaces for data-driven metamaterials design. *Journal of Mechanical Design*, 143(3):031707, 2021.
- [12] Evan W Wang, David Sell, Thaibao Phan, and Jonathan A Fan. Robust design of topology-optimized metasurfaces. *Optical Materials Express*, 9(2):469–482, 2019.
- [13] Sunae So, Jungho Mun, and Junsuk Rho. Simultaneous inverse design of materials and structures via deep learning: demonstration of dipole resonance engineering using core–shell nanoparticles. *ACS applied materials & interfaces*, 11(27):24264–24268, 2019.
- [14] Caglar Gurbuz, Felix Kronawetter, Christoph Dietz, Martin Eser, Jonas Schmid, and Steffen Marburg. Generative adversarial networks for the design of acoustic metamaterials. *The Journal of the Acoustical Society of America*, 149(2):1162–1174, 2021.
- [15] Liwei Wang, Anton van Beek, Daicong Da, Yu-Chin Chan, Ping Zhu, and Wei Chen. Data-driven multiscale design of cellular composites with multiclass microstructures for natural frequency maximization. *Composite Structures*, 280:114949, 2022.

[16] Jun Wang, Daicong Da, Mark Fuge, Rahul Rai, et al. Ih-gan: A conditional generative model for implicit surface-based inverse design of cellular structures. *arXiv preprint arXiv:2103.02588*, 2021.

[17] Liwei Wang, Siyu Tao, Ping Zhu, and Wei Chen. Data-driven topology optimization with multiclass microstructures using latent variable gaussian process. *Journal of Mechanical Design*, 143(3):031708, 2021.

[18] Alex Kulesza and Ben Taskar. Determinantal point processes for machine learning. *arXiv preprint arXiv:1207.6083*, 2012.

[19] Yu-Chin Chan, Daicong Da, Liwei Wang, and Wei Chen. Remixing functionally graded structures: Data-driven topology optimization with multiclass shape blending. *arXiv preprint arXiv:2112.00648*, 2021.

[20] Daicong Da, Yu-Chin Chan, Liwei Wang, and Wei Chen. Data-driven and topological design of structural metamaterials for fracture resistance. *Extreme Mechanics Letters*, 50:101528, 2022.

[21] Liwei Wang, Jagannadh Boddapati, Ke Liu, Ping Zhu, Chiara Daraio, and Wei Chen. Mechanical cloak via data-driven aperiodic metamaterial design, 2021.

[22] Jiaqi Jiang and Jonathan A Fan. Global optimization of dielectric metasurfaces using a physics-driven neural network. *Nano letters*, 19(8):5366–5372, 2019.

[23] Sensong An, Clayton Fowler, Bowen Zheng, Mikhail Y Shalaginov, Hong Tang, Hang Li, Li Zhou, Jun Ding, Anuradha Murthy Agarwal, Clara Rivero-Baleine, et al. A deep learning approach for objective-driven all-dielectric metasurface design. *ACS Photonics*, 6(12):3196–3207, 2019.

[24] Sensong An, Bowen Zheng, Hong Tang, Mikhail Y Shalaginov, Li Zhou, Hang Li, Myungkoo Kang, Kathleen A Richardson, Tian Gu, Juejun Hu, et al. Multifunctional metasurface design with a generative adversarial network. *Advanced Optical Materials*, 9(5):2001433, 2021.

[25] Eric B Whiting, Sawyer D Campbell, Lei Kang, and Douglas H Werner. Meta-atom library generation via an efficient multi-objective shape optimization method. *Optics Express*, 28(16):24229–24242, 2020.

[26] Paula Branco, Luís Torgo, and Rita P Ribeiro. A survey of predictive modeling on imbalanced domains. *ACM Computing Surveys (CSUR)*, 49(2):1–50, 2016.

[27] Ismail Khalid Kazmi, Lihua You, and Jian Jun Zhang. A survey of 2d and 3d shape descriptors. In *2013 10th International Conference Computer Graphics, Imaging and Visualization*, pages 1–10. IEEE, 2013.

[28] Georgios Vamvakas, Basilis Gatos, and Stavros J Perantonis. Handwritten character recognition through two-stage foreground sub-sampling. *Pattern Recognition*, 43(8):2807–2816, 2010.

[29] Zhaocheng Liu, Zhaoming Zhu, and Wenshan Cai. Topological encoding method for data-driven photonics inverse design. *Optics express*, 28(4):4825–4835, 2020.

[30] Diederik P Kingma and Max Welling. Auto-encoding variational bayes. *arXiv preprint arXiv:1312.6114*, 2013.

[31] Martin Philip Bendsoe and Ole Sigmund. *Topology optimization: theory, methods, and applications*. Springer Science & Business Media, 2003.

[32] Liwei Wang, Yu-Chin Chan, Zhao Liu, Ping Zhu, and Wei Chen. Data-driven metamaterial design with laplace-beltrami spectrum as “shape-dna”. *Structural and multidisciplinary optimization*, 61(6), 2020.

[33] Wentai Zhang, Zhangsihao Yang, Haoliang Jiang, Suyash Nigam, Soji Yamakawa, Tomotake Furuhata, Kenji Shimada, and Levent Burak Kara. 3d shape synthesis for conceptual design and optimization using variational autoencoders. In *International Design Engineering Technical Conferences and Computers and Information in Engineering Conference*, volume 59186, page V02AT03A017. American Society of Mechanical Engineers, 2019.

[34] Angela Dai, Charles Ruizhongtai Qi, and Matthias Nießner. Shape completion using 3d-encoder-predictor cnns and shape synthesis. In *Proceedings of the IEEE Conference on Computer Vision and Pattern Recognition*, pages 5868–5877, 2017.

[35] Diederik P Kingma and Jimmy Ba. Adam: A method for stochastic optimization. *arXiv preprint arXiv:1412.6980*, 2014.

[36] Carl Edward Rasmussen. Gaussian processes in machine learning. In *Summer school on machine learning*, pages 63–71. Springer, 2003.

[37] Ramin Bostanabad, Yu-Chin Chan, Liwei Wang, Ping Zhu, and Wei Chen. Globally approximate gaussian processes for big data with application to data-driven metamaterials design. *Journal of Mechanical Design*, 141(11), 2019.

[38] Anton Van Beek, Siyu Tao, Matthew Plumlee, Daniel W Apley, and Wei Chen. Integration of normative decision-making and batch sampling for global metamodeling. *Journal of Mechanical Design*, 142(3):031114, 2020.

[39] Jasper Snoek, Hugo Larochelle, and Ryan P Adams. Practical bayesian optimization of machine learning algorithms. *Advances in neural information processing systems*, 25, 2012.

[40] Mike Gartrell, Ulrich Paquet, and Noam Koenigstein. Bayesian low-rank determinantal point processes. In *Proceedings of the 10th ACM Conference on Recommender Systems*, pages 349–356, 2016.

[41] Wei-Lun Chao, Boqing Gong, Kristen Grauman, and Fei Sha. Large-margin determinantal point processes. In *UAI*, 2015.

[42] Raja Hafiz Affandi, Emily Fox, Ryan Adams, and Ben Taskar. Learning the parameters of determinantal point process kernels. In *International Conference on Machine Learning*, pages 1224–1232. PMLR, 2014.

[43] Alex Kulesza and Ben Taskar. k-dpps: Fixed-size determinantal point processes. In *ICML*, 2011.

[44] Alexei Borodin and Eric M Rains. Eynard–mehta theorem, schur process, and their pfaffian analogs. *Journal of statistical physics*, 121(3):291–317, 2005.

[45] Raja Hafiz Affandi, Alex Kulesza, and Emily B Fox. Markov determinantal point processes. *arXiv preprint arXiv:1210.4850*, 2012.

[46] Mike Gartrell, Ulrich Paquet, and Noam Koenigstein. Low-rank factorization of determinantal point processes. In *Thirty-First AAAI Conference on Artificial Intelligence*, 2017.

[47] Ali Rahimi and Benjamin Recht. Random features for large-scale kernel machines. *Advances in neural information processing systems*, 20, 2007.

[48] Walter Rudin. *Fourier analysis on groups*. Courier Dover Publications, 2017.

[49] Raja Hafiz Affandi, Emily B Fox, and Ben Taskar. Approximate inference in continuous determinantal point processes. *arXiv preprint arXiv:1311.2971*, 2013.

[50] Liang Xia and Piotr Breitkopf. Design of materials using topology optimization and energy-based homogenization approach in matlab. *Structural and multidisciplinary optimization*, 52(6):1229–1241, 2015.

[51] Erik Andreassen and Casper Schousboe Andreassen. How to determine composite material properties using numerical homogenization. *Computational Materials Science*, 83:488–495, 2014.

[52] Jason L Loeppky, Jerome Sacks, and William J Welch. Choosing the sample size of a computer experiment: A practical guide. *Technometrics*, 51(4):366–376, 2009.

[53] Wei-Liem Loh. On latin hypercube sampling. *The annals of statistics*, 24(5):2058–2080, 1996.

[54] Mehdi Mirza and Simon Osindero. Conditional generative adversarial nets. *arXiv preprint arXiv:1411.1784*, 2014.

[55] Kihyuk Sohn, Honglak Lee, and Xinchen Yan. Learning structured output representation using deep conditional generative models. *Advances in neural information processing systems*, 28, 2015.

## Appendix A Data Description

### A.1 2-D Multiclass Shape Blending Dataset

Many existing approaches to multiclass design resort to mutually compatible classes that have been predefined. The setting guarantees seamless alignment across neighbors without frustration, with a substantial compromise of design freedom [19]. To explore beyond the narrow design space, Y. C. Chan *et al.* proposed a novel multiclass blending scheme that produces smoothly graded flexible topologies given a set of baseline classes [19]. Figure. 5(a) provides a visual look at the class remixing developed. A preliminary step is to prepare a set of shape bases whose instances are represented as SDFs. Arbitrary shapes can be produced by a weighted sum of the SDF bases, followed by an activated softmax union that ensures feasibility of the produced topologies and smooth transition across them. Ideally, the basis set is supposed to be as diverse as possible, in terms of both shape and property, so that the resulting functionally graded instances can span even broader coverage. To this end, Y. C. Chan *et al.* harnessed DPP to extract the best 20-size jointly diverse basis set, given a fully observed large-scale dataset [11]. Building on the representative set as well as the class blending method, this work constructs our own dataset named  $\mathcal{D}_{mix}$ . For all the  ${}_{20}C_3 = 1140$  combinations, any of which involves three classes out of the bases, uniform random sampling on  $[0, 1]^3$  generates 50 realizations of the weight parameters, followed by the proposed softmax union across the basis SDFs. This results in  $\mathcal{D}_{mix}$  whose size is  $50 \times 1140 = 57,000$ .

## A.2 2-D Topology Optimization Dataset

TO can be exploited for generating datasets with minimal domain knowledge. The idea was employed when constructing  $\mathcal{D}_{TO}$ ; a set of uniformly distributed 1,000 target properties are sampled in property space, followed by volume-constrained inverse TO that identifies 358 valid structures as initial seeds (see Figure. 5(b) for illustration) [32]. The TO-based library construction offers two distinctive advantages: (i) it guarantees the uniformity of the initial seeds in property space, and (ii) the method is free from human-induced potential bias, often justified as “domain knowledge”. Meanwhile, the TO-based data acquisition possibly suffers from the following issues: (i) it inherits all the limitations of continuum-based TO, such as one-to-many mapping, local optimality and computational overhead; (ii) it is only applicable to the design problems where TO work efficiently; (iii) the optimized topologies without any underlying family could be too scattered in the deep shape space, demanding a larger number of data for DDMD. L. Wang *et al.* addressed most of the challenges by (i) populating the initial 358 shapes with stochastic shape perturbation (Figure. 5(b)) and by (ii) iterative data expansion using the pointwise sampling criterion that promotes both bias reduction and exploration [32]. This resulted in 88,180-size  $\mathcal{D}_{TO}$ . Another version of  $\mathcal{D}_{TO}$  with larger cardinality can be found in L. Wang *et al.* [10].